Geophysical Research Letters

RESEARCH LETTER
10.1029/2018GL081823

Key Points:
- VOC and NO_x emissions affect O_3 peak time oppositely, and O_3 peak time is more sensitive to VOC emissions over the eastern United States
- Simulated O_3 peak value and peak time biases compared to observations indicate the overestimation of biogenic isoprene emissions
- Satellite HCHO columns-derived isoprene emissions corroborate the overestimation of model biogenic isoprene emissions

Supporting Information:
- Supporting Information S1

Correspondence to:
Y. Wang,
yuhang.wang@eas.gatech.edu

Citation:
Li, J., Wang, Y., & Qu, H. (2019). Dependence of summertime surface ozone on NO_x and VOC emissions over the United States: Peak time and value. *Geophysical Research Letters*, *46*. https://doi.org/10.1029/2018GL081823

Received 22 DEC 2018
Accepted 12 MAR 2019
Accepted article online 18 MAR 2019

Dependence of Summertime Surface Ozone on NO_x and VOC Emissions Over the United States: Peak Time and Value

Jianfeng Li[1], Yuhang Wang[1], and Hang Qu[1]

[1]School of Earth and Atmospheric Sciences, Georgia Institute of Technology, Atlanta, GA, USA

Abstract We apply the Regional chEmistry and trAnsport Model to analyze summertime O_3 observations over the contiguous United States. We show that the evaluation of simulated timing of surface ozone maximum with observations provides another independent constraint on the model in addition to O_3 concentrations. Over regions with massive biogenic isoprene emissions,O_3 peak values are sensitive to the emissions of NO_x but not VOCs; however, O_3 peak time is sensitive to isoprene emissions and increasing isoprene emissions leads to earlier peak time. By such relationships and model evaluation with the observations, we find that the underestimation of soil NO_x emissions leads to a low bias of simulated O_3 peak value in the south, while the overestimation of biogenic isoprene emissions results in earlier than observed O_3 peak time in the central, south, and southeast regions. The latter is corroborated by the evaluation using Ozone Monitoring Instrument observations of HCHO tropospheric columns.

Plain Language Summary Surface ozone, which is produced by nitrogen oxides and volatile organic compounds in the daytime, adversely affects human health and vegetation growth. Observed ozone concentrations can be used to evaluate nitrogen oxides and volatile organic compound emissions by using their relationships with ozone concentrations. In this study, we show that the time when ozone reaches its daily maximum (peak time) is also related to nitrogen oxides and volatile organic compound emissions. We use a three-dimensional model to simulate ozone daily maximum concentrations (peak value) and peak time in July 2011 over the contiguous United States. Through model sensitivity analyses, we find that ozone peak values are more sensitive to nitrogen oxide emissions, while ozone peak time is more sensitive to volatile organic compound emissions in the eastern United States. By such relationships and the comparison between observations and model results, we find that the underestimation of soil nitrogen oxides emissions leads to a low bias of simulated ozone peak value in the south, while the overestimation of biogenic isoprene emissions results in earlier than observed ozone peak time in the central, south, and southeast regions. The simulated formaldehyde columns, which are higher than satellite measurements, confirm the latter.

1. Introduction

Surface ozone (O_3), one of the six criteria air pollutants regulated by the U.S. Environmental Protection Agency (EPA), is also a greenhouse gas (Myhre et al., 2013) and can adversely affect human health and vegetation (Glowacz et al., 2015; Jerrett et al., 2009; Li et al., 2017; Turner et al., 2016). O_3 is a secondary pollutant, which is produced by complicated photochemistry reactions with the presence of NO_x ($NO_x = NO + NO_2$) and volatile organic compounds (VOCs; Figure S1 in the supporting information; Liu, Wang, Gu, et al., 2012; Seinfeld & Pandis, 2016). NO_x and VOCs are emitted by both anthropogenic activities (vehicles, power plants, industry, etc.) and natural sources (soil NO_x, lightning NO_x, and biogenic VOCs [BVOCs]). Globally, isoprene emitted by vegetation is the most abundant nonmethane VOC (535 Tg yr^{-1} for the year 2000; Guenther et al., 2012), while anthropogenic NO_x contribute about 75% of the total NO_x emissions (Seinfeld & Pandis, 2016).

The relationship between O_3 production and VOC and NO_x emissions is essential to understand tropospheric chemistry and has been widely studied in recent decades (Cheng et al., 2017; Geng et al., 2008; Liu, Wang, Gu, et al., 2012; Xie et al., 2011). For example, Pierce et al. (1998) examined the sensitivities of O_3 concentrations to isoprene and NO_x emissions in the Regional Acid Deposition Model simulations with different emission scenarios in the eastern United States and found that increased isoprene emissions

produce a shift in elevated O_3 concentrations from VOC sensitivity to NO_x sensitivity over many areas of eastern North America. Gao (2007) analyzed surface O_3 and NO_x diurnal cycles and VOC and NO_x emissions from heavy-duty trucks and low-duty vehicles in California and demonstrated that an O_3 weekend effect with higher O_3 concentrations on weekends compared to weekdays in urban regions is induced by a weekend increase in the ratio of transportation VOC to NO_x emissions, which results from decreased heavy-duty trucks activity relative to low-duty vehicles. Mazzuca et al. (2016) investigated the diurnal variation in the sensitivities of ozone production rate to NO_x and VOCs in September 2013 by using the observations from the NASA Deriving Information on Surface Conditions from COlumn and VERtically Resolved Observations Relavant to Air Quality Houston campaign and the model simulations from a box model and the Community Multiscale Air Quality model. They found that O_3 production shifts from generally being more VOC sensitive in the morning to mainly NO_x sensitive in the afternoon during the campaign. R. Zhang, Cohan, et al. (2017) evaluated the contributions of BVOC emissions to O_3 through Ozone Source Apportionment Technology and brute force zero-out sensitivity tests over the United States and found that BVOCs typically contribute 10%–19% to regional O_3 concentrations at the nonattainment sites during selected O_3 episodes. In general, the O_3-VOC-NO_x relationship can be categorized into two regimes: NO_x-limited regime, where O_3 is more sensitive to NO_x than to VOCs and reducing NO_x emissions is more effective in lowering O_3, and VOC-limited regime, where O_3 is more sensitive to VOCs.

In this study, we investigate a new constraint on the O_3-NO_x-VOC relationship using the sensitivity of O_3 peak time (the time when O_3 reach its maximum in 1 day) to NO_x and VOC emissions, in addition to previously used O_3 concentrations. This new relationship provides another diagnostic of O_3 sensitivity on NO_x and VOC emissions. The observations and modeling of July 2011 over the contiguous United States (CONUS) are analyzed to demonstrate the new O_3-NO_x-VOC relationship and its applications. The Regional chEmical and trAnsport Model (REAM), O_3 surface observations, and other data sets are described in section 2. In section 3, we analyze the dependences of O_3 peak time and the peak value (the maximum hourly concentration of O_3 in 1 day) on NO_x and VOC emissions through sensitivity tests with different emission scenarios. Making use of the dependences, we analyze the discrepancies of O_3 peak time and peak values between REAM simulations and the observations in order to evaluate the emission inventories in the model. Conclusions are given in section 4.

2. Observation Data and Model Description

2.1. Surface Ozone Observations

We obtained O_3 surface concentration measurements in July 2011 from the EPA Air Quality System Data Mart (https://www3.epa.gov/airdata/) and converted them into O_3 peak values and peak time in local time. Data at 1,024 observation sites are available and used in this study. The CONUS was divided into nine regions following the definition of the National Oceanic and Atmospheric Administration (NOAA; http://www.ncdc.noaa.gov/monitoring-references/maps/us-climate-regions.php; Karl & Koss, 1984). Figure 1 shows the regions and the distribution of the O_3 observations sites. There were 185, 63, 196, 146, 148, 30, 134, 77, and 45 sites in central, east north central, northeast, south, southeast, northwest, southwest, west, and west north central, respectively.

2.2. OMI HCHO Tropospheric Vertical Columns

The Ozone Monitoring Instrument (OMI) is an ultraviolet/visible nadir solar backscatter spectrometer on board NASA EOS-Aura Sun-synchronous polar satellite, which was launched in July 2004. It crosses the equator around 13:30 local time. OMI provides tropospheric HCHO column observations with nearly daily global coverage and a nadir spatial resolution of 13 km × 24 km (Levelt et al., 2006). Here we use the newest OMI HCHO version 14 (OMI-v14) level-3 product with a resolution of 0.25° × 0.25° (http://h2co.aeronomie.be/). In the retrieval of OMI-v14, a priori profile shapes extracted from the Intermediate Model of Global Evolution of Species version 2 (IMAGESv2) are used to calculate air mass factors (De Smedt et al., 2015). The IMAGESv2 model reproduces very well observed vertical profiles of HCHO measured during the Intercontinental Chemical Transport Experiment North America (INTEX-A) campaign (July–August 2004) over the U.S. (De Smedt et al., 2015; Stavrakou et al., 2009). Using the HCHO vertical shape from the Compact Atmospheric Multispecies Spectrometer measurements during the SEAC^{4}RS (Studies of

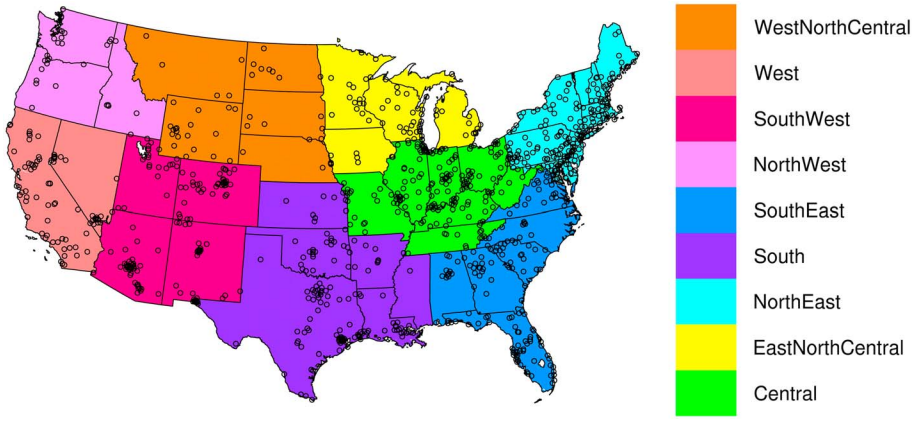

Figure 1. Region definitions and locations of EPA Air Quality System O_3 monitoring sites. Site locations are shown with open circles.

Emissions, Atmospheric Composition, Clouds and Climate Coupling by Regional Surveys) aircraft campaign (August–September 2013) in the OMI-v14 retrieval algorithm, HCHO columns are increased by about 10% in the southeastern U.S. (Zhu et al., 2016). Zhu et al. (2016) suggested that OMI-v14 offers the best estimation of tropospheric HCHO columns in the southeastern U.S. compared to GOME2A-BIRA (V14), GOME2B-BIRA (V14), OMPS-SAO, OMPS-PCA, and OMI-SAO (V003), although OMI-v14 still underestimates the columns by 20% compared to Compact Atmospheric Multispecies Spectrometer-derived HCHO columns. On the other hand, De Smedt et al. (2016) demonstrate that the precision (random error) of OMI-v14 is below 7×10^{14} molecules cm^{-2} in July (which is about 5% for the southeastern U.S.) when considering monthly average columns with a resolution of 20 km × 20 km and that the accuracy (systematic error) of OMI-v14 is about 20% over the southeastern U.S.

HCHO is an intermediate product of isoprene oxidation, and HCHO columns provide a proxy for isoprene emissions (Palmer et al., 2003; Shim et al., 2005). In this study, OMI-v14 HCHO columns are used to evaluate the isoprene emission inventory from the Model of Emissions of Gases and Aerosols from Nature (MEGAN; Guenther et al., 2012).

2.3. Model Description

2.3.1. REAM

REAM has been applied in many tropospheric chemistry and transport studies and emission estimations over East Asia, North America, and polar regions (Alkuwari et al., 2013; Cheng et al., 2017, 2018; Choi, Wang, Yang, et al., 2008; Choi, Wang, Zeng, et al., 2008; Gu et al., 2014, 2013; Koo et al., 2012; Liu et al., 2014; Liu, Wang, Vrekoussis, et al., 2012; Wang et al., 2008; Yang et al., 2011; R. Zhang, Wang, et al., 2017; R. Zhang et al., 2018; Y. Zhang & Wang, 2016; Zhao & Wang, 2009; Zhao et al., 2009, 2010). The model has a horizontal resolution of 36 km × 36 km with 30 vertical layers in the troposphere. Transport is driven by the Weather Research and Forecasting (version 3.6) model-assimilated meteorological fields constrained by the NCEP coupled forecast system model version 2 (CFSv2) products (http://rda.ucar.edu/datasets/ds094.0/; Saha et al., 2011). The chemistry mechanism is from the GEOS-Chem model (v11.01) with updated aerosol uptake of isoprene nitrate based on Fisher et al. (2016). Chemistry boundary conditions and initiations are from a GEOS-Chem simulation with a resolution of 2° × 2.5°. Anthropogenic NO_x, CO, and VOC emissions are from the National Emission Inventory 2011 (NEI2011) provided by the Pacific Northwest National Laboratory. We assume that the weekend emissions are two thirds of the weekday emissions (Choi et al., 2012; Kaynak et al., 2009). This study focuses on weekday analysis, and the weekend emission uncertainty is out of the scope of this study and has little impacts on weekday O_3 peak values and peak time because of the short lifetimes of O_3 and its precursors, VOCs and NO_x. Biogenic VOC emissions are from MEGAN v2.1 (Guenther et al., 2012). Soil-emitted NO_x is calculated by using the Yienger and Levy (YL) scheme (Yienger & Levy, 1995).

2.3.2. MEGAN v2.1

MEGAN (Guenther et al., 2006, 2012) is currently widely used to estimate global and regional BVOC emissions (Fisher et al., 2016; Mao et al., 2013; Stavrakou et al., 2014; Yu et al., 2016). In this study, we use a recommended high-resolution plant functional-type database for the U.S. for the year 2008 (http://lar.wsu.edu/megan/guides.html). Land coverage data are from the GLASS Leaf Area Index (LAI) product with a raw resolution of 0.05° (download from ftp://ftp.glcf.umd.edu/glcf/GLASS/LAI/MODIS/0.05D/), and the GLASS LAI product is derived from MODIS land surface reflectance (MOD09A1; Liang & Xiao, 2012; Xiao et al., 2014). Meteorological parameters, such as temperature, soil moisture, and radiation flux, are from a Weather Research and Forecasting simulation.

3. Results and Discussions

3.1. Dependence of O_3 Peak Values and Time on NO_x and VOCs

To evaluate the dependence of O_3 peak time and values on NO_x and VOC emissions, we made 17 sensitivity simulations with different emission scenarios by using REAM, including STD-REAM where standard anthropogenic and natural NO_x and VOC emissions were used, natural scenarios with varying BVOC or soil NO_x emissions, anthropogenic scenarios with different anthropogenic NO_x or VOC emissions, and combination scenarios where more than two types of emissions were changed. The responses of weekday monthly mean O_3 peak time and peak values to NO_x and VOC emission variations, as well as complete descriptions of the emission scenarios, are illustrated in Figures 2 and S2. Figure 2 shows that the sensitivities of regional O_3 peak time to NO_x and VOC emissions differ significantly from those of O_3 peak values. For example, in central CONUS, O_3 peak time responds to VOC emission changes, while O_3 peak value responds to NO_x emission changes. Therefore, the observations of O_3 peak time provide another set of constraints on model simulations in addition to O_3 peak values (next section). We first discuss the dependence of O_3 peak value on NO_x and VOC emissions.

Generally, anthropogenic NO_x emissions showed positive correlations with regional ozone peak values (Figure 2). The effects of anthropogenic NO_x emissions on peak values were more significant in east north central, central, northeast, south, and southeast than in the other regions. Soil NO_x emissions affect regional O_3 peak values in a manner similar to anthropogenic NO_x emissions. Therefore, the relative importance of the two NO_x sources depends on their relative emission strengths. Soil NO_x dominates in most areas of the western CONUS, while anthropogenic NO_x is predominant in the eastern regions (Figure S3). As a result, increasing soil NO_x emissions by 400% has fewer impacts on O_3 peak values in southeast and northeast than increasing anthropogenic NO_x emissions by 50%, while the two effects are comparable in central and south CONUS. The former has a larger effect in east north central, northwest, southwest, west, and west north central CONUS.

The effects of BVOCs are more apparent than anthropogenic VOCs (Figures 2 and S2). For BVOCs, the correlations between O_3 peak value and emissions are positive in all regions except for in southeast, where a slight decrease is simulated when BVOC emissions are changed by 50%, reflecting the nonlinear O_3 photochemistry in this region of abundant isoprene emissions. Since both VOCs and NO_x show positive correlations with O_3 peak values, concurrent increase (decrease) of NO_x and VOC emissions could elevate (lower) O_3 peak values more as shown by combination sensitivity scenarios in Figure S2. However, it should be noted that O_3 peak values were much more sensitive to NO_x than VOC emissions in east north central, central, northeast, south, and southeast. That is to say, these regions are in NO_x-limited regime, which is consistent with the relatively high BVOC emissions in these areas (Figure S4). In west, west north central, southwest, and northwest, the effects of NO_x and VOC emission changes on O_3 peak values are comparable, but both are significantly weaker than those in the former five regions, due in part to relatively lower NO_x and VOC emissions in these regions and transport factors controlling surface O_3 levels such as stratospheric O_3 intrusion (Langford et al., 2009; Musselman & Korfmacher, 2014).

Figure 2 shows that O_3 peak time is positively correlated with anthropogenic NO_x emissions. As in anthropogenic NO_x, the effects of soil NO_x emissions are generally more significant on O_3 peak values than peak time. VOC emission changes, in general, affect O_3 peak time more than NO_x emissions, but the relationships are somewhat complicated. Generally, O_3 peak time is negatively correlated with BVOC emissions (Figures 2

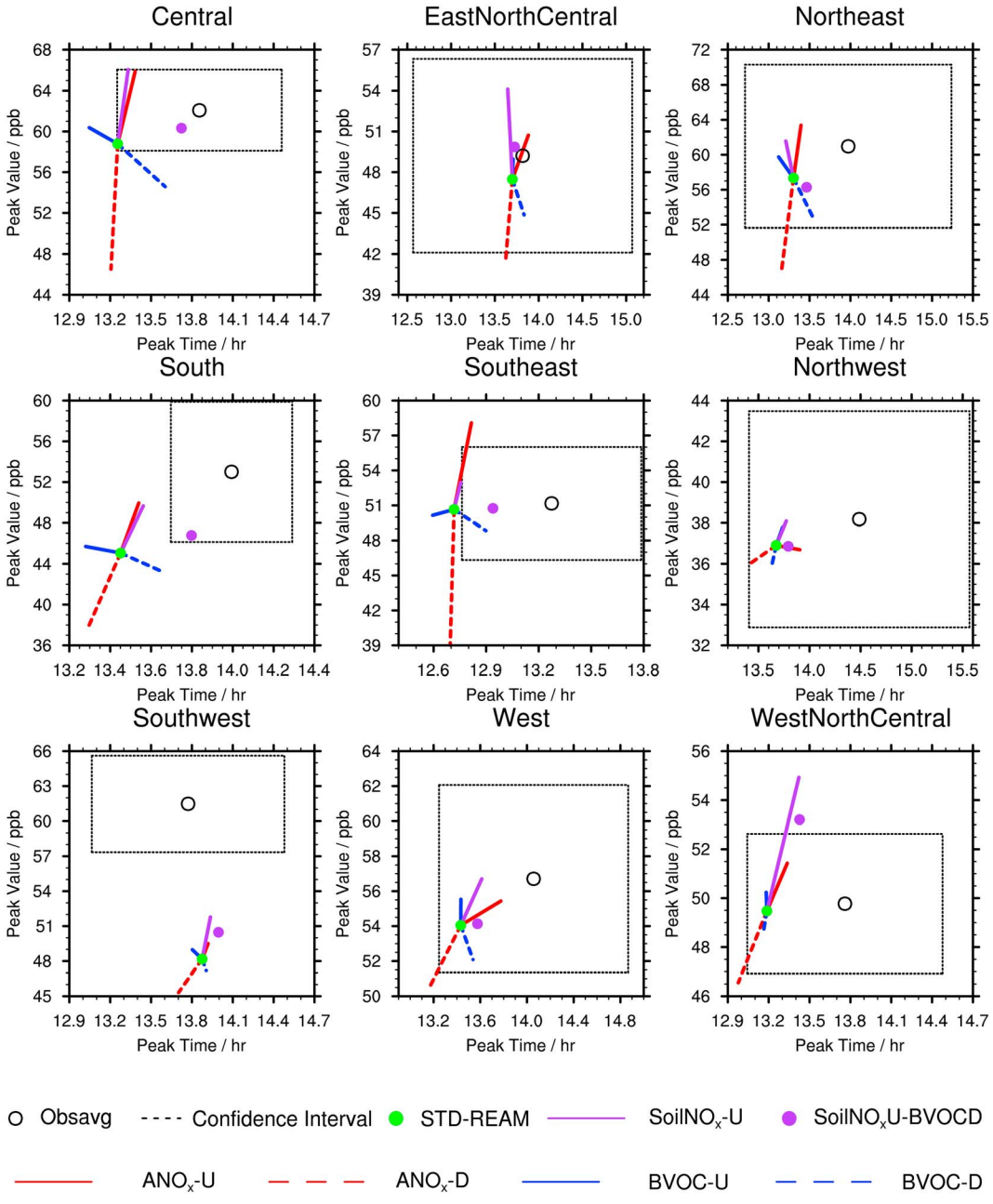

Figure 2. Comparison of weekday monthly mean O_3 peak values and peak time between EPA observations and REAM simulations with different emission scenarios in July 2011 over different regions (Figure 1). *Obsavg* denotes EPA observations. The *confidence interval* box is calculated based on the 99.9% confidence intervals. STD-REAM denotes the standard simulation result without any emission changes. SoilNO_x-U is the sensitivity simulation result after increasing soil NO_x emissions to 5 times. ANO_x-U and ANO_x-D are for increasing and decreasing anthropogenic NO_x by 50%, respectively. BVOC-U and BVOC-D are for increasing and decreasing MEGAN isoprene emissions by 50%, respectively. Soil NO_x U-BVOCD denotes a sensitivity simulation with MEGAN isoprene emissions decreased by 50% and soil NO_x emissions increased to 5 times. Additional sensitivity simulation results are shown in Figure S2.

and S2) in most regions, and it is most significant in central, northeast, south, and southeast, where BVOC emissions are much higher than the other regions (Figure S4). In the other regions, BVOC effects are relatively small. Figure S2 shows that the effects of anthropogenic VOC emissions are also small.

In central, northeast, south, and southeast, O_3 peak value is more sensitive to NO_x emissions but O_3 peak time is more sensitive to VOC (mostly BVOC) emissions (Figure 2). In these regions, O_3 peak time is

negatively correlated with VOC emissions. With sufficient BVOC emissions, it is not surprising that O_3 peak values in the regions are more sensitive to NO_x than VOC emissions. Different sensitivities in O_3 peak time from peak values reflect the O_3 photochemical process (Figure S1). As shown in Figure S5, BVOC and NO_x emissions have opposite impacts on diurnal cycles of NO, RO_2, and HO_2 concentrations: decreasing BVOC emissions decreases HO_2 and RO_2 concentrations and increases NO concentrations, while decreasing NO_x increases HO_2 and RO_2 concentrations and reduces NO concentrations in the morning. Since RO_2 and HO_2 concentrations are changed more significantly than NO concentrations in the early morning, BVOC and NO_x emissions have opposite effects on the daytime O_3 production ($P(O_3) = k_1[RO_2][NO] + k_2[HO_2][NO]$): decreasing BVOC and increasing NO_x emissions shifts the accumulated $P(O_3)$ profile later in time while increasing BVOC and decreasing NO_x emissions shifts the accumulated $P(O_3)$ profile earlier in time.

Figure S5 also shows that the change of BVOC emissions affects accumulated $P(O_3)$ profile more significantly than that of NO_x emissions, especially for decreasing BVOC emissions. The main reason is their different effects on NO concentrations from 5:00 to 8:00 when NO concentrations are changed much more significantly for the NO_x emission sensitivity simulations than for the BVOC emission sensitivity simulations, which partially offsets the changes of RO_2 and HO_2. It reflects the direct impact of NO_x emissions on NO concentrations when photochemistry is weak in the early morning. There is no significant pattern difference for RO_2 and NO_2 concentrations from 5:00 to 13:00 between BVOC and NO_x sensitivity simulations except that (1) decreasing BVOC emissions reduces RO_2 and HO_2 concentrations much more (about 50%) than increasing NO_x emissions, which means that decreasing BVOC emissions shifts accumulated $P(O_3)$ profile much more significantly than increasing NO_x emissions; (2) decreasing NO_x emissions increases RO_2 and HO_2 concentrations some more (about 20%) than increasing BVOC emissions. However, its effect on accumulated $P(O_3)$ profile is canceled out by the effect of NO concentration change difference in the early morning. Therefore, decreasing BVOC emissions and increasing NO_x emissions shift the accumulated $P(O_3)$ profile later in time and delay O_3 peak time, and the sensitivity of O_3 peak time to BVOC emission change is higher than NO_x (Figures S5 and S6).

The sensitivities of O_3 peak time to NO_x and BVOC emissions were also found previously by Lei et al. (2007, 2008). They investigated the sensitivities of O_3 production to NO_x and VOC emissions in April 2003 in the Mexico City Metropolitan Area. Even though Mexico City Metropolitan Area is a VOC-limited region, their sensitivity simulations also showed that O_3 peak shifted to earlier hours with reduced NO_x emissions and later hours with reduced VOC emissions. Therefore, the utilities of the sensitivities of O_3 peak time to NO_x and BVOC emissions discussed in this study are likely extendable to other seasons and regions.

3.2. Application of the O_3-NO_x-VOC Relationships to Evaluate Model VOC and NO_x Emissions

As discussed in the previous section, the sensitivities of O_3 peak values and time to NO_x and VOC emissions are often quite different, therefore providing independent constraints on model simulations. Figure 2 shows that the standard model simulates well on the observed O_3 peak values in most regions but underestimates them in south and southwest. The model generally reproduces O_3 peak time within the 99.9% confidence intervals in most regions except for central, south, and southeast where the simulated O_3 peak time is significantly earlier than the observations.

The large set of sensitivity simulations (Figures 2 and S2) point to possible problems in the model NO_x and BVOC emissions, although the model underestimates of O_3 peak values in the southwest region cannot be easily corrected without increasing soil NO_x emissions by a factor of 10–50, implying that transport of O_3 from the upper troposphere may be underestimated. For the central and southeast regions, observed O_3 peak values are simulated well by the standard model. The relatively high sensitivity of O_3 peak values to NO_x emissions in these regions implies that emissions of NO_x are reasonable. The O_3 peak time simulated by the model, on the other hand, is earlier than the observations. Model sensitivity simulations suggest that O_3 peak time is sensitive to BVOC emissions since anthropogenic VOC emissions are much lower than BVOCs in these regions and reducing BVOC emissions reduces the simulation bias in O_3 peak time.

For the south region, the simulated O_3 peak value is lower and peak time is earlier than the observations, suggesting an increase of NO_x emissions and a decrease of BVOC emissions (Figure 2). It is noteworthy that the underestimation of O_3 peak values mainly occur in the upper south (Figure S7), where soil NO_x

emissions are close or even much higher than anthropogenic NO_x emissions (Figure S3). Several studies demonstrated that the YL scheme underestimated soil NO_x emissions by a factor of 2–4 (Hudman et al., 2012; Jaeglé et al., 2005; Rasool et al., 2016; Wolfe et al., 2015) over the United States. Increasing YL soil NO_x emissions by a factor of 5 brings the simulated regional O_3 peak value closer to the observations, in agreement with the previous studies.

The increase of soil NO_x emissions delays the O_3 peak time. However, the model-simulated O_3 peak time in the south region is still earlier than the observations. Model sensitivity results in Figure 2 suggest that a decrease of BVOC emissions by 50% is necessary. Previous studies showed that MEGAN might overestimate BVOC emissions in some regions of the United States. For example, Wolfe et al. (2015) demonstrated that MEGAN v2.1 overestimated isoprene surface fluxes by up to 40% based on the measurements during the NASA SEAC^{4}RS mission over the Ozarks. Carlton and Baker (2011) indicated that MEGAN v2.04 led to much higher isoprene concentrations than the surface and aloft measurements in July 1998 in the Ozarks region. Top-down constraints from satellite HCHO measurements, such as OMI, provide an independent means to evaluate the bottom-up isoprene emissions from MEGAN, although the HCHO yield from isoprene oxidation could lead to some uncertainties (Marais et al., 2012). In the next section, we examine the simulated isoprene emissions based on OMI HCHO column measurements.

Our evaluation of the NEI2011 NO_x emissions is consistent with the results by Salmon et al. (2018), who examined the NO_x/CO_2, CO/CO_2, and CO/NO_x ratios in February–March 2015 over the northeastern United States and found that NO_x emissions from NEI2011 and NEI2014 were in agreement with the aircraft observation-derived emissions. Cheng et al. (2017) also found good agreement between model simulations and aircraft observations of O_3, NO_x, and VOCs in July 2011 around the Washington-Baltimore area. However, Canty et al. (2015), Travis et al. (2016), and Anderson et al. (2014) suggested that on-road mobile sources in the NEI NO_x emission inventories were overestimated by around 50%–70% in 2007 and 2011, while Dallmann and Harley (2010) suggested that on-road mobile NO_x emissions from NEI2005 were 15% lower than fuel-derived on-road NO_x emissions. The different evaluations of NEI NO_x emissions might be caused by the limitations of the data sets used to assess the NEI emissions, such as the temporal-spatial coverage of measurements, which would bias the evaluations due to significant inhomogeneity of NO_x emissions (Marr et al., 2013), measurement uncertainties, and differences in evaluation methods.

3.3. Constraints of OMI-v14 Tropospheric HCHO Column Measurements on Isoprene Emissions

Figure 3a shows the monthly average of STD-REAM tropospheric HCHO columns at 12:30–14:30 LT in July 2011. The corresponding regridded OMI-v14 HCHO columns based on the model resolution are shown in Figure 3b. The relative difference (REAM/OMI-1) is shown in Figure 3c. STD-REAM captured the spatial distribution of HCHO columns ($R^2 = 0.62$) with high column concentrations in central, south, and southeast where there are dense forests. However, STD-REAM simulates much higher columns than OMI-v14 in these regions. Over the model grid cells where surface O_3 observation sites are available in central, south, and southeast, the STD-REAM tropospheric HCHO columns are about 36.9% higher than the corresponding OMI-v14 columns on average, and 29.7%, 37.8%, and 46.0% for central, south, and southeast, respectively.

HCHO is mainly produced during the oxidation of biogenic isoprene, and HCHO column observations from space are highly specific to biogenic isoprene in central, south, and southeast (Millet et al., 2008; Shim et al., 2005). A quantified relationship between biogenic isoprene emissions and HCHO tropospheric columns at 12:00–15:00 LT was derived by Millet et al. (2008):

$$\Omega_{\mathrm{HCHO}} = 2.40\ E_{\mathrm{ISOPRENE}} + 0.51 \tag{1}$$

where Ω_{HCHO} denotes tropospheric HCHO columns in 10^{16} molecules cm^{-2} and $\mathrm{E_{ISOPRENE}}$ denotes biogenic isoprene emissions in 10^{13} atoms C cm^{-2} s^{-1}. Therefore, the top-down constraint on an a priori emission inventory can be calculated by

$$\Delta\Omega_{\mathrm{HCHO}} = 2.40\ \Delta E_{\mathrm{ISOPRENE}} \tag{2}$$

In order to reduce the smearing effect (Millet et al., 2008), we regridded 36 km × 36 km data to a resolution of 1° × 1°. If we only included those grids containing, the observation sites in central, south, and southeast,

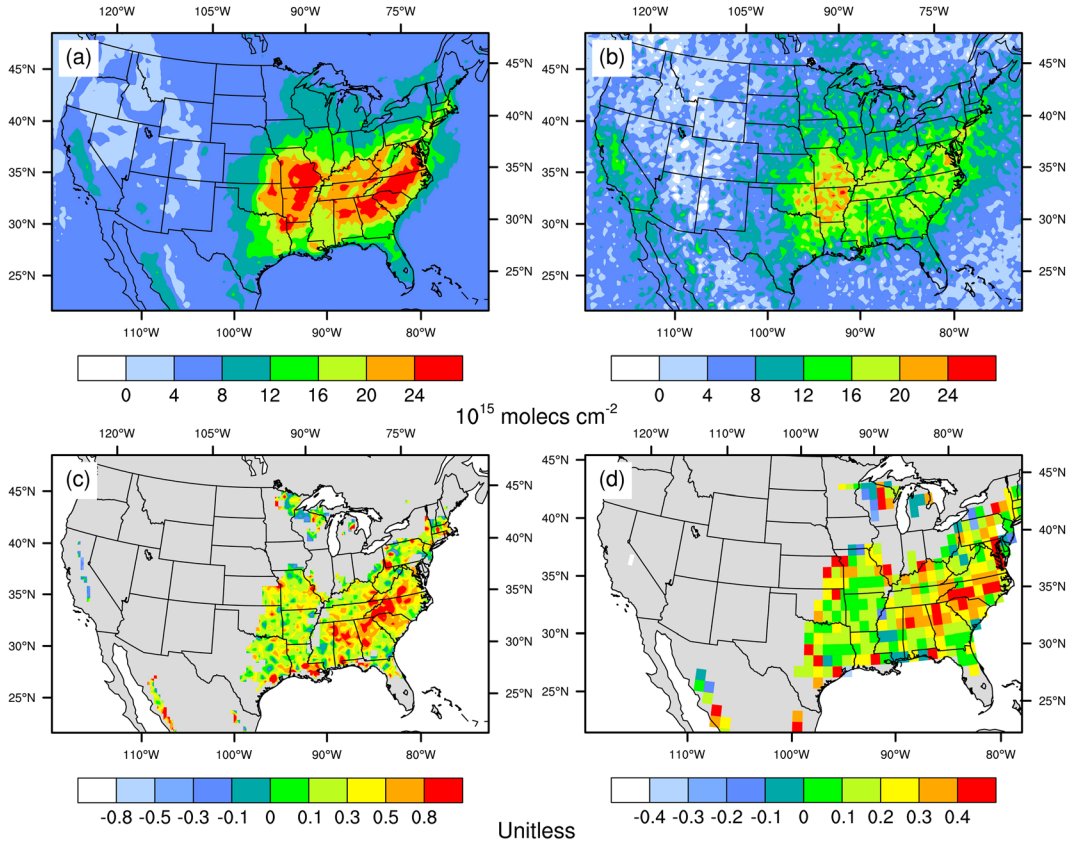

Figure 3. Spatial distribution of (a) tropospheric HCHO vertical columns of STD-REAM between 12:30 and 14:30 LT, (b) tropospheric HCHO vertical columns of OMI-v14 retrievals, (c) relative difference between STD-REAM and OMI-v14 (REAM/OMI-1), and (d) the relative difference of the MEGAN isoprene emissions from those derived from OMI-v14 HCHO column data for regions with MEGAN isoprene emissions $>3 \times 10^{12}$ atoms C cm^{-2} s^{-1}. All data shown are monthly averages for July 2011.

STD-REAM tropospheric HCHO column were 31.5% or 0.41×10^{16} molecules cm^{-2} higher than OMI-v14 on average, corresponding to a biogenic isoprene emission bias of 1.71×10^{12} atoms C cm^{-2} s^{-1}. As a result, the MEGAN isoprene emissions are overestimated by 27.2% on average in these regions and 30.4%, 21.3%, and 28.9% for central, south, and southeast, respectively. Figure 3d shows the distribution of the factional overestimation of isoprene emissions. These results are consistent with Millet et al. (2008), who suggested that isoprene emissions derived from OMI HCHO columns were 23% lower than MEGAN from June to August, and the absolute differences were the largest in the Ozark Plateau, the Upper South and Southeast where MEGAN overestimation could reach up to about 50%. Accounting for the uncertainty of OMI HCHO columns of ~25%, we estimate that the overestimation of MEGAN isoprene emissions in July 2011 is in the range of 5.6%–48.6% in central, south, and southeast, which provides additional support to the previous results on the basis of model-simulated peak O_3 time and values in comparison to the observations for these regions.

4. Conclusions

We evaluated the dependence of O_3 peak values and time on NO_x and VOC emissions through model simulations with different emission scenarios in July 2011 over the CONUS. In addition to the previously known dependence of O_3 peak values on NO_x and VOC emissions, we find that O_3 peak time is affected by NO_x and VOC emissions in a different manner. As such, the observations of O_3 peak values and time provide useful constraints on model emissions of NO_x and VOCs. Over regions with extensive biogenic isoprene emissions, such as the central, south, southeast, and northeast regions, the O_3 peak values are sensitive to the emissions

of NO_x but not VOCs. However, O_3 peak time in these regions is sensitive to isoprene emissions, where an increase of isoprene emissions leads to earlier peak time of surface O_3.

We applied these O_3 dependences to analyze REAM performance on reproducing the observations of surface O_3 peak values and time in July 2011 over the CONUS. REAM reproduced well O_3 peak values and peak time in most regions except in the south and southwest, where peak values were significantly underestimated, and in the central, south, and southeast, where peak time was earlier than observed. The underestimation of soil NO_x emissions from the Yienger and Levy (YL) scheme could be the reason for the O_3 peak value underestimation in the south. However, it is insufficient to explain the low bias of O_3 peak value in the southwest, suggesting an underestimation of O_3 transport from the upper troposphere. The earlier than observed O_3 peak time in the central, south, and southeast was attributed to an overestimation of biogenic isoprene emissions by MEGAN, which was consistent with the estimate of a 27.1% $\pm$ 21.5% overestimation of isoprene emissions in these regions in July 2011 on the basis of OMI HCHO column observations. As our study is limited in July 2011 over the CONUS, evaluations of O_3 peak time and value sensitivities to NO_x and VOC emissions are needed for other seasons and regions. Given the sensitivities found in this study for the summertime, we recommend that the dependence of O_3 peak time on NO_x and VOC emissions be applied to evaluate model emissions in conjunction with the often used evaluation of O_3 concentrations.

Acknowledgments
This work was supported by the NASA ACMAP Program. We thank Yuzhong Zhang and Jenny Fisher for providing the updated GEOS-Chem chemistry mechanism files and Yuzhong Zhang and Ziming Ke for discussions with J. Li. O_3 surface concentration measurements are from the EPA Air Quality System (AQS) Data Mart (https://www3.epa.gov/airdata/). OMI HCHO tropospheric columns are from a website http://h2co.aeronomie.be. CFSv2 data sets are from http://rda.ucar.edu/datasets/ds094.0/. The GLASS Leaf Area Index (LAI) product can be accessed via ftp://ftp.glcf.umd.edu/glcf/GLASS/LAI/MODIS/0.05D/. Archived model outputs for standard and sensitivity simulations are available on https://www.dropbox.com/sh/axi7vbvtm6x0wp4/AACwH2PGDkr8yYnbMHYv7Hzua?dl=0.

References

Alkuwari, F. A., Guillas, S., & Wang, Y. (2013). Statistical downscaling of an air quality model using Fitted Empirical Orthogonal Functions. *Atmospheric Environment*, *81*, 1–10. https://doi.org/10.1016/j.atmosenv.2013.08.031

Anderson, D. C., Loughner, C. P., Diskin, G., Weinheimer, A., Canty, T. P., Salawitch, R. J., et al. (2014). Measured and modeled CO and NO_y in DISCOVER-AQ: An evaluation of emissions and chemistry over the eastern US. *Atmospheric Environment*, *96*, 78–87. https://doi.org/10.1016/j.atmosenv.2014.07.004

Canty, T., Hembeck, L., Vinciguerra, T., Goldberg, D., Carpenter, S., Allen, D., et al. (2015). Ozone and NO_x chemistry in the eastern US: Evaluation of CMAQ/CB05 with satellite (OMI) data. *Atmospheric Chemistry and Physics*, *15*(19), 10,965–10,982. https://doi.org/10.5194/acp-15-10965-2015

Carlton, A. G., & Baker, K. R. (2011). Photochemical modeling of the Ozark isoprene volcano: MEGAN, BEIS, and their impacts on air quality predictions. *Environmental Science & Technology*, *45*(10), 4438–4445. https://doi.org/10.1021/es200050x

Cheng, Y., Wang, Y., Zhang, Y., Chen, G., Crawford, J. H., Kleb, M. M., et al. (2017). Large biogenic contribution to boundary layer O_3-CO regression slope in summer. *Geophysical Research Letters*, *44*, 7061–7068. https://doi.org/10.1002/2017GL074405

Cheng, Y., Wang, Y., Zhang, Y., Crawford, J. H., Diskin, G. S., Weinheimer, A. J., & Fried, A. (2018). Estimator of surface ozone using formaldehyde and carbon monoxide concentrations over the eastern United States in summer. *Journal of Geophysical Research: Atmospheres*, *123*, 7642–7655. https://doi.org/10.1029/2018JD028452

Choi, Y., Kim, H., Tong, D., & Lee, P. (2012). Summertime weekly cycles of observed and modeled NO_x and O_3 concentrations as a function of satellite-derived ozone production sensitivity and land use types over the continental United States. *Atmospheric Chemistry and Physics*, *12*(14), 6291–6307. https://doi.org/10.5194/acp-12-6291-2012

Choi, Y., Wang, Y., Yang, Q., Cunnold, D., Zeng, T., Shim, C., et al. (2008). Spring to summer northward migration of high O_3 over the western North Atlantic. *Geophysical Research Letters*, *35*, L04818. https://doi.org/10.1029/2007GL032276

Choi, Y., Wang, Y., Zeng, T., Cunnold, D., Yang, E. S., Martin, R., et al. (2008). Springtime transitions of NO_2, CO, and O_3 over North America: Model evaluation and analysis. *Journal of Geophysical Research*, *113*, D20311. https://doi.org/10.1029/2007JD009632

Dallmann, T. R., & Harley, R. A. (2010). Evaluation of mobile source emission trends in the United States. *Journal of Geophysical Research*, *115*, D14305. https://doi.org/10.1029/2010JD013862

De Smedt, I., Stavrakou, T., Hendrick, F., Danckaert, T., Vlemmix, T., Pinardi, G., et al. (2015). Diurnal, seasonal and long-term variations of global formaldehyde columns inferred from combined OMI and GOME-2 observations. *Atmospheric Chemistry and Physics Discussions*, *15*(21), 12,519–12,545. https://doi.org/10.5194/acp-15-12519-2015

De Smedt, I., N. Theys, H. Yu, T. Danckaert, J. Van Gent, &M. Van Roozendael (2016).S5P/TROPOMI HCHO ATBD *Rep. 1.0.0*, 65 pp.

Fisher, J. A., Jacob, D. J., Travis, K. R., Kim, P. S., Marais, E. A., Chan Miller, C., et al. (2016). Organic nitrate chemistry and its implications for nitrogen budgets in an isoprene-and monoterpene-rich atmosphere: Constraints from aircraft ($SEAC^4RS$) and ground-based (SOAS) observations in the southeast US. *Atmospheric Chemistry and Physics*, *16*(9), 5969–5991. https://doi.org/10.5194/acp-16-5969-2016

Gao, H. O. (2007). Day of week effects on diurnal ozone/NO_x cycles and transportation emissions in Southern California. *Transportation Research Part D: Transport and Environment*, *12*(4), 292–305. https://doi.org/10.1016/j.trd.2007.03.004

Geng, F., Tie, X., Xu, J., Zhou, G., Peng, L., Gao, W., et al. (2008). Characterizations of ozone, NO_x, and VOCs measured in Shanghai, China. *Atmospheric Environment*, *42*(29), 6873–6883. https://doi.org/10.1016/j.atmosenv.2008.05.045

Glowacz, M., Colgan, R., & Rees, D. (2015). Influence of continuous exposure to gaseous ozone on the quality of red bell peppers, cucumbers and zucchini. *Postharvest Biology and Technology*, *99*, 1–8. https://doi.org/10.1016/j.postharvbio.2014.06.015

Gu, D., Wang, Y., Smeltzer, C., & Boersma, K. F. (2014). Anthropogenic emissions of NO_x over China: Reconciling the difference of inverse modeling results using GOME-2 and OMI measurements. *Journal of Geophysical Research: Atmospheres*, *119*, 7732–7740. https://doi.org/10.1002/2014JD021644

Gu, D., Wang, Y., Smeltzer, C., & Liu, Z. (2013). Reduction in NO_x emission trends over China: Regional and seasonal variations. *Environmental Science & Technology*, *47*(22), 12,912–12,919. https://doi.org/10.1021/es401727e

Guenther, A. B., Jiang, X., Heald, C. L., Sakulyanontvittaya, T., Duhl, T., Emmons, L. K., & Wang, X. (2012). The Model of Emissions of Gases and Aerosols from Nature version 2.1 (MEGAN2.1): An extended and updated framework for modeling biogenic emissions. *Geoscientific Model Development*, *5*, 1471–1492. https://doi.org/10.5194/gmd-5-1471-2012

Guenther, A. B., Karl, T., Harley, P., Wiedinmyer, C., Palmer, P. I., & Geron, C. (2006). Estimates of global terrestrial isoprene emissions using MEGAN (Model of Emissions of Gases and Aerosols from Nature). *Atmospheric Chemistry and Physics*, *6*(11), 3181–3210. https://doi.org/10.5194/acp-6-3181-2006

Hudman, R. C., Moore, N. E., Mebust, A. K., Martin, R. V., Russell, A. R., Valin, L. C., & Cohen, R. C. (2012). Steps towards a mechanistic model of global soil nitric oxide emissions: Implementation and space based-constraints. *Atmospheric Chemistry and Physics*, *12*(16), 7779–7795. https://doi.org/10.5194/acp-12-7779-2012

Jaeglé, L., Steinberger, L., Martin, R. V., & Chance, K. (2005). Global partitioning of NO_x sources using satellite observations: Relative roles of fossil fuel combustion, biomass burning and soil emissions. *Faraday Discussions*, *130*, 407–423. https://doi.org/10.1039/B502128F

Jerrett, M., Burnett, R. T., Pope, C. A. III, Ito, K., Thurston, G., Krewski, D., et al. (2009). Long-term ozone exposure and mortality. *New England Journal of Medicine*, *360*(11), 1085–1095. https://doi.org/10.1056/NEJMoa0803894

Karl, T., & Koss, W. J. (1984). *Regional and national monthly, seasonal, and annual temperature weighted by area, 1895–1983*, *Historical climatology series* (Vol. 4-3). Asheville, N.C: National Climatic Data Center.

Kaynak, B., Hu, Y., Martin, R. V., Sioris, C. E., & Russell, A. G. (2009). Comparison of weekly cycle of NO_2 satellite retrievals and NO_x emission inventories for the continental United States. *Journal of Geophysical Research*, *114*, D05302. https://doi.org/10.1029/2008JD010714

Koo, J.-H., Wang, Y., Kurosu, T. P., Chance, K., Rozanov, A., Richter, A., et al. (2012). Characteristics of tropospheric ozone depletion events in the Arctic spring: Analysis of the ARCTAS, ARCPAC, and ARCIONS measurements and satellite BrO observations. *Atmospheric Chemistry and Physics*, *12*(20), 9909–9922. https://doi.org/10.5194/acp-12-9909-2012

Langford, A. O., Aikin, K. C., Eubank, C. S., & Williams, E. J. (2009). Stratospheric contribution to high surface ozone in Colorado during springtime. *Geophysical Research Letters*, *36*, L12801. https://doi.org/10.1029/2009GL038367

Lei, W., de Foy, B., Zavala, M., Volkamer, R., & Molina, L. T. (2007). Characterizing ozone production in the Mexico City Metropolitan Area: A case study using a chemical transport model. *Atmospheric Chemistry and Physics*, *7*(5), 1347–1366. https://doi.org/10.5194/acp-7-1347-2007

Lei, W., Zavala, M., de Foy, B., Volkamer, R., & Molina, L. T. (2008). Characterizing ozone production and response under different meteorological conditions in Mexico City. *Atmospheric Chemistry and Physics*, *8*(24), 7571–7581. https://doi.org/10.5194/acp-8-7571-2008

Levelt, P. F., van den Oord, G. H. J., Dobber, M. R., Malkki, A., Visser, H., de Vries, J., et al. (2006). The ozone monitoring instrument. *IEEE Transactions on Geoscience and Remote Sensing*, *44*(5), 1093–1101. https://doi.org/10.1109/TGRS.2006.872333

Li, S., Harley, P. C., & Niinemets, Ü. (2017). Ozone-induced foliar damage and release of stress volatiles is highly dependent on stomatal openness and priming by low-level ozone exposure in Phaseolus vulgaris. *Plant, Cell & Environment*, *40*(9), 1984–2003. https://doi.org/10.1111/pce.13003

Liang, S., & Xiao, Z. (2012). Global land surface products: Leaf area index product data collection (1985–2010), Beijing Normal University, https://doi.org/10.6050/glass863.3004.db

Liu, Z., Wang, Y., Costabile, F., Amoroso, A., Zhao, C., Huey, L. G., et al. (2014). Evidence of aerosols as a media for rapid daytime HONO production over China. *Environmental Science & Technology*, *48*(24), 14386–14391. https://doi.org/10.1021/es504163z

Liu, Z., Wang, Y., Gu, D., Zhao, C., Huey, L. G., Stickel, R., et al. (2012). Summertime photochemistry during CAREBeijing-2007: RO_x budgets and O_3 formation. *Atmospheric Chemistry and Physics*, *12*(16), 7737–7752. https://doi.org/10.5194/acp-12-7737-2012

Liu, Z., Wang, Y., Vrekoussis, M., Richter, A., Wittrock, F., Burrows, J. P., et al. (2012). Exploring the missing source of glyoxal (CHOCHO) over China. *Geophysical Research Letters*, *39*, L10812. https://doi.org/10.1029/2012GL051645

Mao, J., Paulot, F., Jacob, D. J., Cohen, R. C., Crounse, J. D., Wennberg, P. O., et al. (2013). Ozone and organic nitrates over the eastern United States: Sensitivity to isoprene chemistry. *Journal of Geophysical Research: Atmospheres*, *118*, 11,256–211,268. https://doi.org/10.1002/jgrd.50817

Marais, E. A., Jacob, D. J., Kurosu, T. P., Chance, K., Murphy, J. G., Reeves, C., et al. (2012). Isoprene emissions in Africa inferred from OMI observations of formaldehyde columns. *Atmospheric Chemistry and Physics*, *12*(14), 6219–6235. https://doi.org/10.5194/acp-12-6219-2012

Marr, L. C., Moore, T. O., Klapmeyer, M. E., & Killar, M. B. (2013). Comparison of NO_x fluxes measured by eddy covariance to emission inventories and land use. *Environmental Science & Technology*, *47*(4), 1800–1808. https://doi.org/10.1021/es303150y

Mazzuca, G. M., Ren, X., Loughner, C. P., Estes, M., Crawford, J. H., Pickering, K. E., et al. (2016). Ozone production and its sensitivity to NO_x and VOCs: Results from the DISCOVER-AQ field experiment, Houston 2013. *Atmospheric Chemistry and Physics*, *16*(22), 14,463–14,474. https://doi.org/10.5194/acp-16-14463-2016

Millet, D. B., Jacob, D. J., Boersma, K. F., Fu, T. M., Kurosu, T. P., Chance, K., et al. (2008). Spatial distribution of isoprene emissions from North America derived from formaldehyde column measurements by the OMI satellite sensor. *Journal of Geophysical Research*, *113*, D02307. https://doi.org/10.1029/2007JD008950

Musselman, R. C., & Korfmacher, J. L. (2014). Ozone in remote areas of the Southern Rocky Mountains. *Atmospheric Environment*, *82*, 383–390. https://doi.org/10.1016/j.atmosenv.2013.10.051

Myhre, G., Shindell, D., Bréon, F.-M., Collins, W., Fuglestvedt, J., Huang, J., et al. (2013). Anthropogenic and natural radiative forcing. In T. F. Stocker, et al. (Eds.), *Climate change 2013: The Physical Science Basis. Contribution of Working Group I to the Fifth Assessment Report of the Intergovernmental Panel on Climate Change* (pp. 659–740). Cambridge, United Kingdom and New York, NY, USA: Cambridge University Press.

Palmer, P. I., Jacob, D. J., Fiore, A. M., Martin, R. V., Chance, K., & Kurosu, T. P. (2003). Mapping isoprene emissions over North America using formaldehyde column observations from space. *Journal of Geophysical Research*, *108*(D6), 4180. https://doi.org/10.1029/2002JD002153

Pierce, T., Geron, C., Bender, L., Dennis, R., Tonnesen, G., & Guenther, A. (1998). Influence of increased isoprene emissions on regional ozone modeling. *Journal of Geophysical Research*, *103*(D19), 25,611–25,629. https://doi.org/10.1029/98JD01804

Rasool, Q. Z., Zhang, R., Lash, B., Cohan, D. S., Cooter, E. J., Bash, J. O., & Lamsal, L. N. (2016). Enhanced representation of soil NO emissions in the Community Multiscale Air Quality (CMAQ) model version 5.0.2. *Geoscientific Model Development*, *9*(9), 3177–3197. https://doi.org/10.5194/gmd-9-3177-2016

Saha, S., S. Moorthi, X. Wu, J. Wang, S. Nadiga, P. Tripp, et al. (2011), NCEP climate forecast system version 2 (CFSv2) 6-hourly products, edited, Research Data Archive at the National Center for Atmospheric Research, Computational and Information Systems Laboratory. https://doi.org/10.5065/D61C1TXF

Salmon, O., Shepson, P., Ren, X., He, H., Hall, D., Dickerson, R., et al. (2018). Top-down estimates of NO_x and CO emissions from Washington, DC-Baltimore during the WINTER campaign. *Journal of Geophysical Research: Atmospheres*, *123*, 7705–7724. https://doi.org/10.1029/2018JD028539

Seinfeld, J. H., & Pandis, S. N. (2016). *Atmospheric chemistry and physics: From air pollution to climate change*. Hoboken, NJ: John Wiley.

Shim, C., Wang, Y., Choi, Y., Palmer, P. I., Abbot, D. S., & Chance, K. (2005). Constraining global isoprene emissions with Global Ozone Monitoring Experiment (GOME) formaldehyde column measurements. *Journal of Geophysical Research*, *110*, D24301. https://doi.org/10.1029/2004JD005629

Stavrakou, T., Müller, J.-F., Bauwens, M., De Smedt, I., Van Roozendael, M., Guenther, A., et al. (2014). Isoprene emissions over Asia 1979–2012: Impact of climate and land-use changes. *Atmospheric Chemistry and Physics*, *14*(9), 4587–4605. https://doi.org/10.5194/acp-14-4587-2014

Stavrakou, T., Müller, J.-F., De Smedt, I., Roozendael, M. V., Van Der Werf, G., Giglio, L., & Guenther, A. (2009). Evaluating the performance of pyrogenic and biogenic emission inventories against one decade of space-based formaldehyde columns. *Atmospheric Chemistry and Physics*, *9*(3), 1037–1060. https://doi.org/10.5194/acp-9-1037-2009

Travis, K. R., Jacob, D. J., Fisher, J. A., Kim, P. S., Marais, E. A., Zhu, L., et al. (2016). Why do models overestimate surface ozone in the Southeast United States? *Atmospheric Chemistry and Physics*, *16*(21), 13,561–13,577. https://doi.org/10.5194/acp-16-13561-2016

Turner, M. C., Jerrett, M., Pope, C. A. III, Krewski, D., Gapstur, S. M., Diver, W. R., et al. (2016). Long-term ozone exposure and mortality in a large prospective study. *American Journal of Respiratory and Critical Care Medicine*, *193*(10), 1134–1142. https://doi.org/10.1164/rccm.201508-1633OC

Wang, Y., Choi, Y., Zeng, T., Davis, D., Buhr, M., Huey, L. G., & Neff, W. (2008). Assessing the photochemical impact of snow NO_x emissions over Antarctica during ANTCI 2003. *Atmospheric Environment*, *41*(19), 3944–3958. https://doi.org/10.1016/j.atmosenv.2007.01.056.

Wolfe, G. M., Hanisco, T. F., Arkinson, H. L., Bui, T. P., Crounse, J. D., Dean-Day, J., et al. (2015). Quantifying sources and sinks of reactive gases in the lower atmosphere using airborne flux observations. *Geophysical Research Letters*, *42*, 8231–8240. https://doi.org/10.1002/2015GL065839

Xiao, Z., Liang, S., Wang, J., Chen, P., Yin, X., Zhang, L., & Song, J. (2014). Use of general regression neural networks for generating the GLASS leaf area index product from time-series MODIS surface reflectance. *IEEE Transactions on Geoscience and Remote Sensing*, *52*(1), 209–223. https://doi.org/10.1109/TGRS.2013.2237780

Xie, Y., Elleman, R., Jobson, T., & Lamb, B. (2011). Evaluation of O_3-NO_x-VOC sensitivities predicted with the CMAQ photochemical model using Pacific Northwest 2001 field observations. *Journal of Geophysical Research*, *116*, D20303. https://doi.org/10.1029/2011JD015801

Yang, Q., Wang, Y., Zhao, C., Liu, Z., Gustafson, W. I. Jr., & Shao, M. (2011). NO_x emission reduction and its effects on ozone during the 2008 Olympic Games. *Environmental Science & Technology*, *45*(15), 6404–6410. https://doi.org/10.1021/es200675v

Yienger, J. J., & Levy, H. (1995). Empirical model of global soil-biogenic NO_x emissions. *Journal of Geophysical Research*, *100*(D6), 11447–11,464. https://doi.org/10.1029/95JD00370

Yu, K., Jacob, D. J., Fisher, J. A., Kim, P. S., Marais, E. A., Miller, C. C., et al. (2016). Sensitivity to grid resolution in the ability of a chemical transport model to simulate observed oxidant chemistry under high-isoprene conditions. *Atmospheric Chemistry and Physics*, *16*(7), 4369–4378. https://doi.org/10.5194/acp-16-4369-2016

Zhang, R., Cohan, A., Biazar, A. P., & Cohan, D. S. (2017). Source apportionment of biogenic contributions to ozone formation over the United States. *Atmospheric Environment*, *164*, 8–19. https://doi.org/10.1016/j.atmosenv.2017.05.044

Zhang, R., Wang, Y., He, Q., Chen, L., Zhang, Y., Qu, H., et al. (2017). Enhanced trans-Himalaya pollution transport to the Tibetan Plateau by cut-off low systems. *Atmospheric Chemistry and Physics*, *17*(4), 3083–3095. https://doi.org/10.5194/acp-17-3083-2017

Zhang, R., Wang, Y., Smeltzer, C., Qu, H., Koshak, W., & Boersma, K. F. (2018). Comparing OMI-based and EPA AQS in situ NO_2 trends: Towards understanding surface NO_x emission changes. *Atmospheric Measurement Techniques*, *11*(7), 3955–3967. https://doi.org/10.5194/amt-11-3955-2018

Zhang, Y., & Wang, Y. (2016). Climate-driven ground-level ozone extreme in the fall over the Southeast United States. *Proceedings of the National Academy of Sciences*, *113*(36), 10,025–10,030. https://doi.org/10.1073/pnas.1602563113

Zhao, C., & Wang, Y. (2009). Assimilated inversion of NO_x emissions over East Asia using OMI NO_2 column measurements. *Geophysical Research Letters*, *36*, L06805. https://doi.org/10.1029/2008GL037123

Zhao, C., Wang, Y., Choi, Y., & Zeng, T. (2009). Summertime impact of convective transport and lightning NO_x production over North America: Modeling dependence on meteorological simulations. *Atmospheric Chemistry and Physics*, *9*(13), 4315–4327. https://doi.org/10.5194/acp-9-4315-2009

Zhao, C., Wang, Y., Yang, Q., Fu, R., Cunnold, D., & Choi, Y. (2010). Impact of East Asian summer monsoon on the air quality over China: View from space. *Journal of Geophysical Research*, *115*, D09301. https://doi.org/10.1029/2009JD012745

Zhu, L., Jacob, D. J., Kim, P. S., Fisher, J. A., Yu, K., Travis, K. R., et al. (2016). Observing atmospheric formaldehyde (HCHO) from space: Validation and intercomparison of six retrievals from four satellites (OMI, GOME2A, GOME2B, OMPS) with SEAC^{4}RS aircraft observations over the southeast US. *Atmospheric Chemistry and Physics*, *16*(21), 13,477–13,490. https://doi.org/10.5194/acp-16-13477-2016